

RealRestorer: Towards Generalizable Real-World Image Restoration with Large-Scale Image Editing Models

Yufeng Yang^{1,2} Xianfang Zeng^{2,†} Zhangqi Jiang² Fukun Yin² Jianzhuang Liu³ Wei Cheng²
 Jinghong Lan² Shiyu Liu² Yuqi Peng³ Gang Yu^{2,‡} Shifeng Chen^{3,4,‡}

¹Southern University of Science and Technology ²StepFun

³Shenzhen Institutes of Advanced Technology, Chinese Academy of Sciences ⁴Shenzhen University of Advanced Technology

[🏠 Project Page](#) [👤 Models](#) [👤 RealIR-Bench](#) [🔗 Code](#)

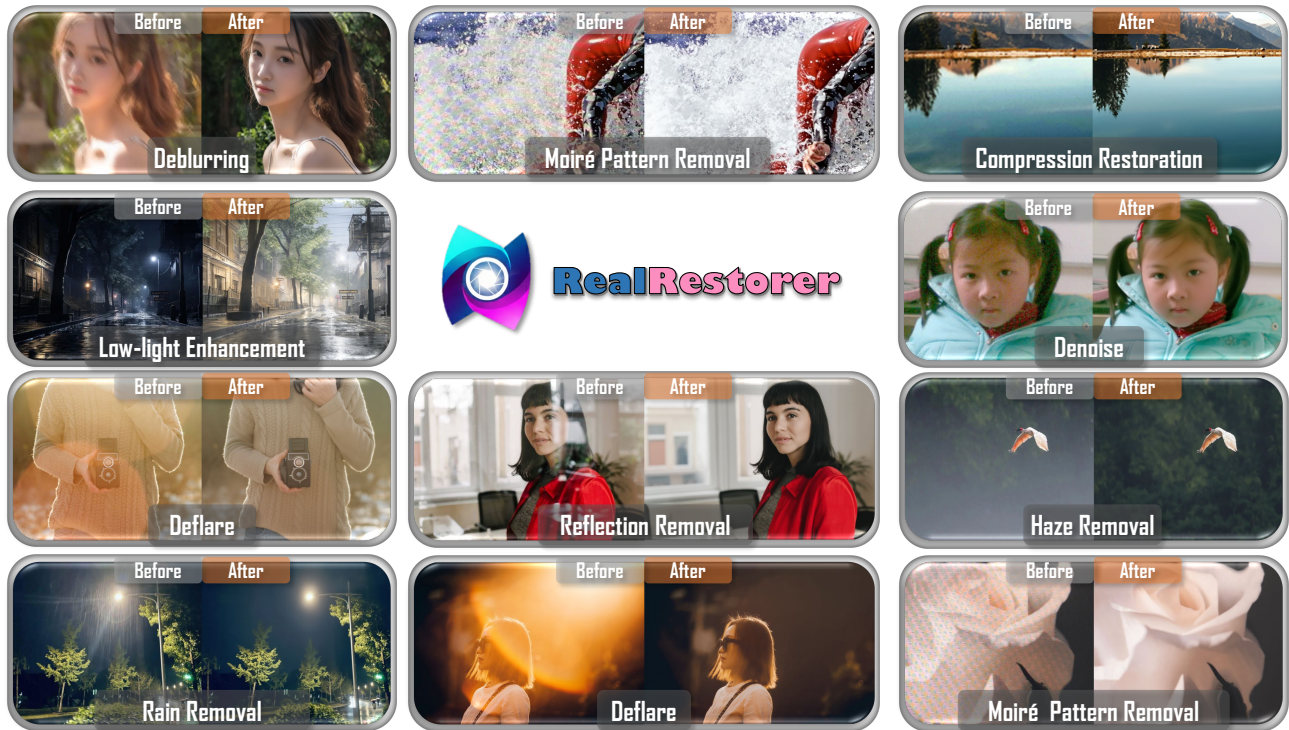


Figure 1. RealRestorer effectively restores diverse real-world image degradations, including deblurring, moiré pattern removal, compression restoration, reflection removal, hazing removal, rain removal, deflare, and low-light enhancement.

Abstract

Image restoration under real-world degradations is critical for downstream tasks such as autonomous driving and object detection. However, existing restoration models are often limited by the scale and distribution of their training data, resulting in poor generalization to real-world scenarios. Recently, large-scale image editing models have shown strong generalization ability in restoration tasks, especially for closed-source models like Nano Banana Pro, which can restore images while preserving consistency. Nev-

ertheless, achieving such performance with those large universal models requires substantial data and computational costs. To address this issue, we construct a large-scale dataset covering nine common real-world degradation types and train a state-of-the-art open-source model to narrow the gap with closed-source alternatives. Furthermore, we introduce RealIR-Bench, which contains 464 real-world degraded images and tailored evaluation metrics focusing on degradation removal and consistency preservation. Extensive experiments demonstrate our model ranks first among open-source methods, achieving state-of-the-art performance.

[†] leads this project; [‡]Corresponding authors.

1. Introduction

Image restoration [15, 31, 35, 37, 70] aims to recover high-quality images from degraded observations and serves as a fundamental building block for downstream applications such as autonomous driving [4, 23], remote sensing [62], detection [22, 27], and 3D reconstruction [68]. However, real-world images often suffer from diverse and co-existing degradations [1, 3, 10, 11, 13, 16, 19, 21, 25, 26, 36, 40, 60, 71], including blur, rain, noise, low-light, moiré patterns, haze, compression artifacts, reflection, and flare. This complexity goes beyond the single degradation and single model paradigm.

To address this, recent all-in-one restoration methods [24, 33, 48, 69] attempt to handle multiple degradations within a unified framework. Nevertheless, they often rely on a limited set of synthetic degradation distributions, while collecting large-scale real degraded-clean pairs remains expensive and difficult. As a result, these models can generalize poorly to real-world scenarios. In parallel, large image editing models trained on massive editing datasets have recently demonstrated strong restoration capabilities [74], such as Nano Banana Pro [56] and GPT-Image-1.5 [45]. However, these models are typically trained with closed-source data and compute, which makes them hard to reproduce and limits their utility for the research community. Despite this, leveraging the strong priors learned by image editing models provides a promising path to overcome the key limitation of traditional restoration approaches.

However, conventional restoration datasets often focus on a narrow degradation distribution that is not representative of real-world conditions. Evaluation protocols that emphasize only reference-based metrics further exacerbate this issue, as they may not reflect perceptual quality, robustness across diverse degradations, or detail consistency in real scenes.

To bridge these gaps, we design a comprehensive degradation synthesis pipeline to generate high-quality training data, aiming to narrow the gap between synthetic and real-world degradations. Based on this dataset, we fine-tune an open-source image editing model **RealRestorer** across nine restoration tasks, and further introduce a new benchmark **RealIR-Bench** to evaluate restoration performance under real-world degradations.

In summary, our contributions are threefold:

- We develop **RealRestorer**, an open-source real-world image restoration model that sets a new state of the art and achieves performance highly comparable to closed-source systems. We will release the model to facilitate future research in real-world restoration.
- We propose a data generation pipeline to produce high-quality restoration training data with diverse and representative degradations. This pipeline provides a valuable resource for developing more robust restoration models.
- We develop a new benchmark, **RealIR-Bench**, grounded

in real-world cases, to evaluate both degradation restoration and consistency preservation. By addressing the lack of reliable evaluation protocols for real-world restoration, it enables more authentic and comprehensive assessment of restoration models.

2. Related Work

2.1. Single-Degradation Restoration

Single-degradation restoration methods typically focus on removing one specific type of degradation under constrained and well-defined scenarios. With the rapid development of deep learning, numerous works [5, 24, 32, 44, 73] have achieved impressive performance on individual tasks such as deblurring, haze removal, low-light enhancement, deflare, and reflection removal. These approaches often rely on carefully designed architectures and degradation-specific priors, enabling strong performance.

However, most single-degradation models are built upon task-specific assumptions, where the degradation type is pre-defined and relatively homogeneous, which makes models trained for a single degradation tend to generalize poorly and may even introduce secondary artifacts when encountering unseen or compound degradations.

Moreover, many existing methods are trained and evaluated primarily on synthetic datasets with simplified degradation models, which may not faithfully represent the complexity of real-world data distributions. This gap between synthetic training data and real-world testing scenarios further limits their robustness and practical applicability. Consequently, while single-degradation methods achieve strong performance on benchmark datasets, their effectiveness in real-world applications remains constrained.

2.2. All-in-One Image Restoration

All-in-one approaches [7, 17, 33, 34, 38, 42, 48, 69] aim to handle multiple degradations within a unified network by balancing shared representations and task-specific components. Nevertheless, many of these methods still rely heavily on synthetic datasets with limited and overly simplified degradation patterns. Such a narrow training distribution often results in weak robustness and poor generalization to real-world degradations, where corruption characteristics are diverse, complex, and domain-dependent.

Meanwhile, large diffusion or flow-matching image editing models [12, 39, 46, 53] have recently demonstrated strong semantic priors for image enhancement and restoration. Trained on massive image-text pairs, these image editing models [30, 41, 57, 65] can leverage semantic conditioning and often generalize better to real-world data than small specialized restoration networks. Therefore, transferring and exploiting the priors of large image editing models

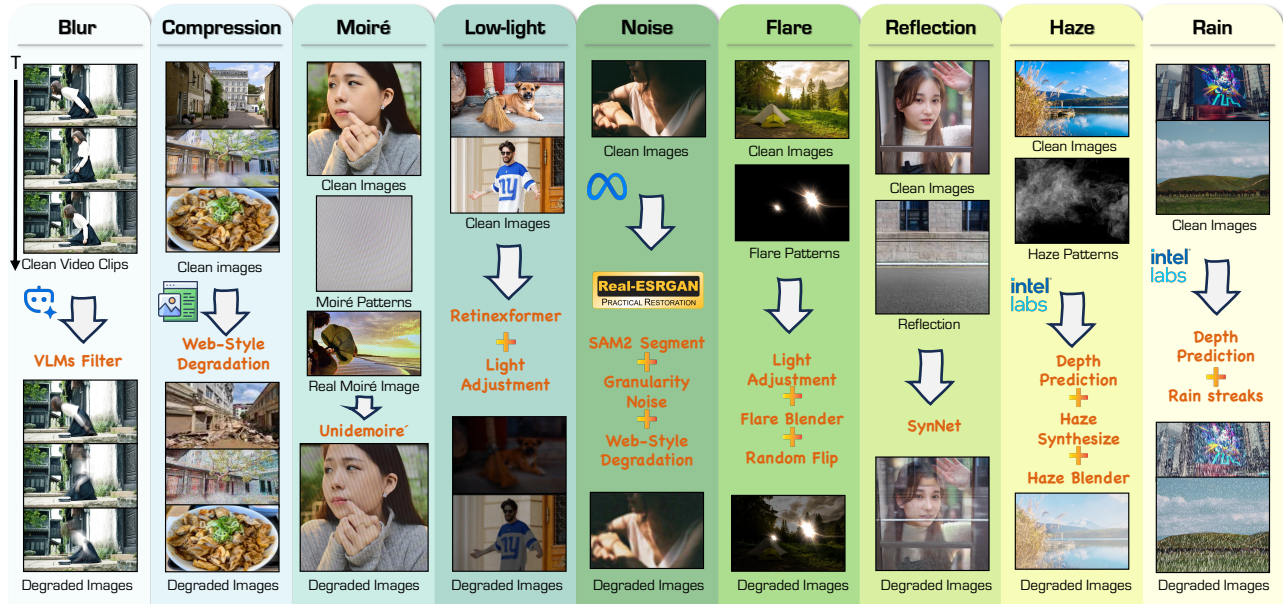


Figure 2. Overview of our large-scale Synthetic Degradation Data pipeline. We construct nine representative degradation types, including blur, compression artifacts, moiré patterns, low-light, noise, flare, reflection, haze, and rain. Compared with previous synthetic-only pipelines, our upgraded framework incorporates granular noise modeling, segment-aware perturbations, and web-style degradation processes, significantly narrowing the gap between synthetic and real-world distributions. This comprehensive pipeline enables more robust and generalizable restoration learning.

provides a promising direction for building restoration systems with stronger real-world generalization.

Motivated by this observation, we develop a high-quality and realistic degradation synthesis pipeline covering nine major degradations and use it to fine-tune open-source image editing models for robust real-world restoration while maintaining strong content consistency. Furthermore, to evaluate real-world restoration performance in the absence of clean references, we curate a benchmark of 464 real images spanning nine single-degradation categories, and propose new evaluation metrics that measure both degradation removal ability and consistency with the input content. Based on the proposed dataset and metrics, our fine-tuned model achieves state-of-the-art performance among open-source methods and is competitive with closed-source systems, while qualitative results further demonstrate strong generalization to real-world degradations.

3. RealRestorer

3.1. Data Construction

Existing image restoration datasets [17, 34] often rely on a single degradation model to synthesize degraded images and use a fixed composition strategy to explicitly disentangle degradation features for representation learning. These modeling approaches are effective for specific degradation settings. However, in real-world scenarios, degradations are far more complex and diverse. Simple synthetic degradation models are usually insufficient to approximate real degrada-

tion distributions, and they are often not robust enough for large-scale training that aims at strong generalization.

To address this limitation, we develop a new dataset collection pipeline that produces more realistic degradation patterns while keeping the paired clean images highly consistent with their degraded counterparts.

In general, we adopt two main ways to obtain high-quality paired data for image restoration of nine tasks:

Synthetic Degradation Data: Start from clean images and synthesize degradations. This approach is highly scalable as long as sufficient clean images can be collected from the internet. However, even with increasingly sophisticated degradation synthesis, it remains challenging to fully capture the diversity and complexity of real-world degradations. Nevertheless, such synthetic data can still be valuable, as it provides a convenient way to transfer general image editing priors to image restoration models and helps them acquire foundational restoration knowledge. We leverage several powerful open-source models to support the synthetic data generation process, including SAM-2 [52], and MiDaS [51]. These models are used to filter unsuitable samples and provide essential structural and geometric information required for realistic degradation synthesis, such as semantic masks and depth cues.

In our pipeline, to ensure high data quality, we employ the Vision-Language Models (VLMs) and quality assessment models [43] to filter out low-quality or unsuitable images like watermarked images. After forming pairs, we further

examine the degree of degradation alignment between the degraded and restored images to ensure that the degradation patterns are learnable from the paired data. Specifically, the synthetic pairing data construction is illustrated as follows.

Blur: The motion blur dataset is primarily synthesized using temporal averaging over video clips to simulate realistic motion trajectories. Both the target and source images are filtered to ensure consistent blur patterns. In addition, web-style degradation, including common blur operations, such as Gaussian blur and standard motion blur, is incorporated to better approximate real-world motion blur characteristics.

Compression Artifacts: We simulate compression artifacts using JPEG compression and image resizing to approximate common web compression effects. In addition to standard JPEG degradation, we also incorporate web-style compression processes to better reflect the wide range of compression artifacts found in online images.

Moiré Patterns: Following UniDemoiré [67], we generate 3,000 moiré patterns at multiple scales and randomly fuse one to three patterns into clean images. This strategy substantially improves the diversity and generalization capability of the model for moiré pattern removal.

Low-Light: We simulate low-light conditions by applying brightness attenuation and gamma correction to reduce pixel intensity. Moreover, we train a separate model [5] using paired datasets such as LOL [66] and LSRW [18], reversing the low-exposure and high-exposure image pairs. This trained model is then applied to clean images to better mimic realistic low-light distributions.

Noise: We adopt web-style degradation as the primary noise synthesis pipeline. Compared with the degradation strategy used in Real-ESRGAN [61], we further introduce granular noise for web images. Additionally, we incorporate segment-aware noise, which significantly improves performance on real-world denoising tasks.

Flare: We collect more than 3,000 glare patterns and adapt them to clean images for realistic blending. In addition, random horizontal and vertical flipping is applied to further enhance the diversity of the generated data pairs.

Reflection: For reflection degradation synthesis, we collect two sources of clean images. The first source mainly consists of portrait images, which are treated as transmission layers. The second source contains diverse scenes with human faces, which are used as reflection layers. To increase the diversity of the paired data, we randomly swap a few portions of the image pairs, using human portraits as reflection layers instead of transmission layers. The overall synthesis pipeline follows SynNet [64].

Haze: We synthesize hazy images based on the classic atmospheric scattering model by estimating depth from clean images and generating fog accordingly [20]. To better simulate real haze, we collect nearly 200 haze patterns and randomly blend them with the synthesized haze, making the

results closer to real-world haze distributions.

Rain: To synthesize realistic rain degradation, we not only add rain streaks but also incorporate splashes and simulate physical effects such as perspective distortion and droplet sputtering. Furthermore, we collect 200 real rain patterns and randomly blend them into clean images to enhance diversity and realism. Besides, we also adopt the rain category from the FoundIR dataset [34], which contains about 70K paired samples.

Real-World Degradation Data: Collect real degraded images and generate corresponding clean images by removing degradations using high performance restoration models. Compared with synthetic pairing, this approach is more likely to preserve the true degradation statistics of real-world data, enabling restoration models trained on such pairs to generalize better to real scenarios. To bridge the gap between synthetic and real-world degradations, we collect real degraded images from the web and pair them with high-quality references.

During web data collection, we first employ the CLIP model [49] to filter images based on degradation-related semantic cues. While this approach effectively removes a portion of irrelevant samples, it still introduces noisy cases, such as watermarked images or visually similar but non-degraded content. To further refine the dataset, we apply a watermark detection filter and leverage Qwen3-VL-8B-Instruct [58] to assess and verify the degree of degradation. After generating clean references using high-performance image generation models, we further examine the consistency of the paired data by employing low-level metrics to detect potential content shifts. A subset of the filtered pairs is then manually reviewed to ensure that the degradation type and severity are properly aligned between degraded inputs and their corresponding clean references. These curated real-world degradation samples enable the model to better adapt its parameters to realistic data distributions. Such adaptation helps the model converge more effectively toward real-world scenarios, consistent with prior findings in large-scale generative modeling [47, 57, 59].

Additional details and qualitative demonstrations are provided in Appendix A.

3.2. Method and Training Strategy

We fine-tune the base model Step1X-Edit [41] built on a large Diffusion in Transformer (DiT) backbone [46], which is effective for generation. It is equipped with QwenVL [2] as a text encoder that injects high-level semantic extraction into the DiT denoising pathway. Inside the diffusion network, a dual-stream design is used to jointly process semantic information together with noise and the conditional input image. The reference image and output image are both encoded into latent space by Flux-VAE [29]. During training, all the components are initialized from the officially released

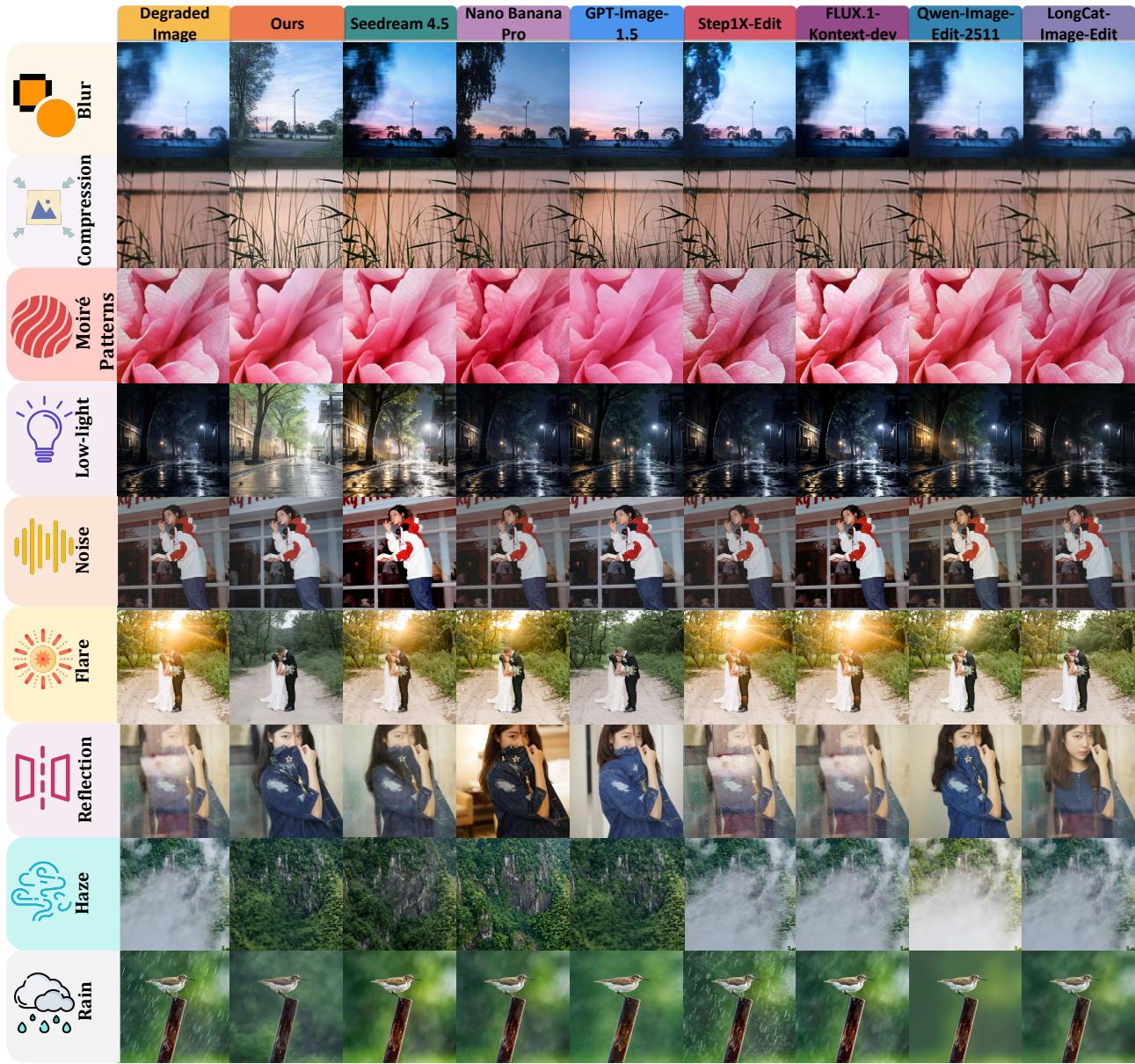


Figure 3. Comparison with state-of-the-art image editing models across nine real-world degradations, including blur, compression artifacts, moiré patterns, low-light, noise, flare, reflection, haze, and rain. We compare our method with large-scale image editing models, such as Seedream 4.5, Nano Banana Pro, GPT-Image-1.5, Step1X-Edit, FLUX.1-Kontext-dev, Qwen-Image-Edit-2511, and LongCat-Image-Edit.

checkpoint of Step1X-Edit, and we freeze the Flux-VAE and text encoder, only fine-tune the DiT. Starting from the original image editing model, we fine-tune on nine restoration tasks in two stages: a Transfer-training stage for large-scale restoration transfer and a Supervised Fine-tuning stage for constraining the manifold of the final model distribution.

Transfer Training Stage: In the first stage, we use synthetic paired data to transfer high-level knowledge and priors from image editing to image restoration. Since we initialize from a pretrained backbone, we eschew progressive resolution schedules [41] for training. Instead, we adopt a high-

resolution setting of 1024×1024 throughout the entire training process. The learning rate is kept constant at $1e^{-5}$, and the global batch size is set to 16. Since most of our training data has a resolution higher than 1024×1024 , no additional upsampling is required, which helps preserve fine-grained details and maintain training stability. For each degradation of nine, we adopt single and fixed prompts, which are also the same for the second training stage. For multi-task learning, we adopt an average sampling ratio across all tasks during training. After several steps of transfer training, **Real-Restorer** begins to exhibit signs of knowledge transfer from

high-level image editing tasks to image restoration tasks, which is insufficient in the base model.

Although **RealRestorer** gradually acquires the basic capability to handle simple degradation patterns across all nine tasks, its ability to distinguish and model diverse real-world degradation patterns remains limited. In particular, the model still struggles to capture fine-grained details in complex scenarios. In some cases, noticeable artifacts are present, and the model fails to respond effectively to certain types of degradations. This observation motivates us to introduce a second training stage aimed at improving generalization and restoration quality under real-world degradation scenarios. Moreover, we observe that different task types exhibit distinct learning dynamics and require varying training durations. Therefore, we select a balanced trade-off checkpoint at the end of the first stage to preserve both generation capability and cross-task generalization.

Supervised Fine-tuning Stage: For the second training stage, we incorporate real-world degradation data to further enhance restoration fidelity and improve generalization under real-world degradation scenarios [57, 59, 65]. Compared with the first stage, this stage emphasizes adaptation to complex and authentic degradation patterns. We adopt a cosine annealing learning rate schedule, where the learning rate is gradually decayed to zero, using the same initial learning rate as in the first stage. This smooth decay strategy stabilizes the transition between training stages and encourages the model to progressively adapt to the real-to-clean paired data. By gradually reducing the optimization step size, the model is guided to converge toward a parameter configuration that better aligns with the distribution represented by the high-quality real-world dataset, thereby improving restoration fidelity and robustness under realistic degradations.

Importantly, instead of completely replacing synthetic data, we adopt a **Progressively-Mixed** training strategy, which retains a small proportion of synthetic paired samples during the second stage. **RealRestorer** is first exposed to diverse synthetic degradations to build broad generalization, and then gradually adapted to real-world degradations while maintaining exposure to synthetic distributions. Such a hybrid curriculum helps prevent overfitting to specific real degradation patterns and preserves cross-task robustness. More detailed discussions and quantitative analyses of this training strategy are provided in the ablation study. In addition, we introduce a web-style degradation data augmentation strategy throughout the training process to enhance robustness to images collected from the web. Such images typically suffer from low visual quality, compression artifacts, and other degradations. By simulating these practical degradation patterns during training, the model becomes better equipped to handle real-world inputs and produce better restoration results under challenging conditions.

Throughout the two-stage training process, we select the

intermediate checkpoint with the best generalization capability to maintain a balanced performance across multiple tasks and ensure strong overall performance of the final model. All our experiments are conducted on 8 NVIDIA H800 GPUs. More implementation details can be found in Appendix B.

4. Benchmark and Evaluation

4.1. RealIR-Bench

Traditional image restoration benchmarks primarily focus on single-degradation tasks with synthetic corruptions or limited degradation patterns, which makes them insufficient for evaluating model performance in real-world applications [14, 17, 34, 50]. Such benchmarks often fail to capture the complexity, diversity, and unpredictability of degradations encountered in practical scenarios.

To properly evaluate restoration performance under real-world degradations, we construct a new benchmark composed entirely of internet-sourced, naturally degraded images. The proposed benchmark spans nine common restoration tasks and covers a wide range of degradation types frequently observed in real-world photography, including blur, rain, noise, low-light, moiré patterns, haze, compression artifacts, reflection, and flare, which collectively represent the most common forms of real-world image degradation. To preserve the authentic real-world degradation distribution, we directly curate images from web sources rather than synthesizing degradations. We further conduct manual filtering to ensure both quality control and diversity across degradation types, scene content, and severity levels. This human-in-the-loop curation process helps preserve realistic degradation characteristics while avoiding overly biased, repetitive, or low-quality samples. By combining automatic collection with manual verification, we ensure that the benchmark better reflects the complexity and diversity of degradations encountered in real-world scenarios, rather than artifacts introduced by purely synthetic construction.

In total, the benchmark contains 464 non-reference degraded images for testing. To ensure a fair and consistent evaluation protocol, we adopt a fixed enhancement instruction for all samples. This design minimizes the influence of instruction variation and allows the evaluation to focus more directly on a model’s restoration capability and its ability to preserve image consistency.

The collected images cover a variety of common real-world degradation scenarios, including complex and mixed degradations that are often challenging for restoration models. As a result, the benchmark provides a practical and demanding testbed for assessing real-world restoration performance. More details about the benchmark construction and data statistics are provided in Appendix C.

Table 1. Quantitative comparison on the Rain Removal, Deblurring, Low-light Enhancement, Haze Removal, and Reflection Removal tasks. We compared state-of-the-art (SOTA) image editing models. For each task, we reported LPS (\downarrow), RS (\uparrow), and FS (\uparrow). The best result is marked in **bold**, and underline indicates the second-best result. The **best** and **second-best** open-source results are highlighted with yellow and blue backgrounds, respectively.

Method	Open-source	Rain Removal			Deblurring			Low-light Enhancement			Haze Removal			Reflection Removal		
		LPS \downarrow	RS \uparrow	FS \uparrow	LPS \downarrow	RS \uparrow	FS \uparrow	LPS \downarrow	RS \uparrow	FS \uparrow	LPS \downarrow	RS \uparrow	FS \uparrow	LPS \downarrow	RS \uparrow	FS \uparrow
<i>Image Editing Methods</i>																
Nano Banana Pro [56]	No	0.429	<u>2.063</u>	0.236	0.326	1.068	0.144	0.467	0.720	0.077	0.492	1.920	0.195	0.358	1.368	0.176
GPT-Image-1.5 [45]	No	0.535	2.120	<u>0.197</u>	0.532	<u>1.667</u>	<u>0.156</u>	0.523	<u>1.048</u>	<u>0.100</u>	0.558	<u>1.840</u>	<u>0.163</u>	0.468	2.320	0.247
Seedream 4.5 [55]	No	0.438	1.500	0.169	0.254	0.255	0.038	0.423	0.600	0.069	0.418	1.140	0.133	0.291	1.156	0.164
LongCat-Image-Edit [57]	Yes	0.381	<u>1.302</u>	<u>0.161</u>	0.200	0.000	0.000	0.158	0.120	0.020	0.236	0.000	0.000	0.254	1.060	0.158
Qwen-Image-Edit-2511 [65]	Yes	0.435	1.736	0.196	<u>0.170</u>	0.240	0.040	<u>0.122</u>	0.080	0.014	0.337	0.060	0.008	0.333	<u>1.820</u>	<u>0.243</u>
FLUX.1-Kontext-dev [30]	Yes	0.244	0.673	0.102	0.090	0.104	0.019	0.108	0.160	0.029	0.058	0.020	0.004	0.048	0.127	0.024
Step1X-Edit [41]	Yes	<u>0.282</u>	0.019	0.003	0.321	<u>0.906</u>	<u>0.123</u>	0.306	<u>0.340</u>	<u>0.047</u>	<u>0.194</u>	0.190	0.031	<u>0.247</u>	0.080	0.012
RealRestorer (ours)	Yes	0.371	1.076	0.135	0.582	1.900	0.159	0.597	1.360	0.110	0.339	0.680	0.090	0.290	<u>1.620</u>	<u>0.230</u>

Table 2. Quantitative comparison on the Deflare, Demoiré, Denoise, and Compression-restoration tasks. The average results of all 9 tasks are reported in the last column. We compared state-of-the-art (SOTA) image editing models. For each task, we reported LPIPS (\downarrow), RS (\uparrow), and FS (\uparrow). The best result is marked in **bold**, and underline indicates the second-best result. The **best** and **second-best** open-source results are highlighted with yellow and blue backgrounds, respectively.

Method	Open-source	Deflare			Moiré Patterns Removal			Denoise			Compression Restoration			Avg Total (9)		
		LPS \downarrow	RS \uparrow	FS \uparrow	LPS \downarrow	RS \uparrow	FS \uparrow	LPS \downarrow	RS \uparrow	FS \uparrow	LPS \downarrow	RS \uparrow	FS \uparrow	LPS \downarrow	RS \uparrow	FS \uparrow
<i>Image Editing Methods</i>																
Nano Banana Pro [56]	No	0.214	1.222	0.192	0.562	1.560	0.137	<u>0.386</u>	0.712	0.087	0.483	1.122	0.116	0.413	1.306	0.153
GPT-Image-1.5 [45]	No	0.336	1.415	0.188	0.646	<u>1.633</u>	0.116	0.496	0.993	0.100	0.633	1.167	0.086	0.525	1.578	<u>0.150</u>
Seedream 4.5 [54]	No	0.225	1.104	0.171	0.548	1.600	0.145	0.387	0.770	<u>0.094</u>	0.529	<u>1.136</u>	<u>0.107</u>	0.390	1.029	0.125
LongCat-Image-Edit [57]	Yes	0.241	1.717	0.261	<u>0.420</u>	1.200	<u>0.139</u>	0.350	0.471	0.061	0.188	0.083	0.014	<u>0.270</u>	0.661	0.097
Qwen-Image-Edit-2511 [65]	Yes	0.222	<u>1.660</u>	<u>0.258</u>	0.595	1.660	0.135	0.429	<u>0.824</u>	<u>0.094</u>	<u>0.242</u>	0.300	0.046	0.320	<u>0.931</u>	<u>0.127</u>
FLUX.1-Kontext-dev [30]	Yes	0.064	0.264	0.049	0.348	0.540	0.070	0.429	0.628	0.072	0.429	<u>0.628</u>	<u>0.072</u>	0.202	0.349	0.056
Step1X-Edit [41]	Yes	<u>0.173</u>	0.000	0.000	0.654	0.410	0.028	<u>0.409</u>	0.098	0.012	0.344	0.383	0.050	0.325	0.270	0.036
RealRestorer (ours)	Yes	0.239	1.623	0.247	0.563	<u>1.620</u>	<u>0.142</u>	0.478	<u>0.863</u>	<u>0.090</u>	0.547	1.067	0.097	0.445	<u>1.312</u>	0.146

4.2. Experimental Results on RealIR-Bench

Based on RealIR-Bench, we evaluate a diverse set of large image editing models’ ability in image restoration towards the real world, covering state-of-the-art closed-source systems such as GPT-Image-1.5 [45], Nano Banana Pro [56], Seedream 4.5 [55], as well as strong open models including Qwen-Image-Edit-2511 [65], FLUX.1-Kontext-dev [30], LongCat-Image-Edit [57] and Step1X-Edit [41]. We provide nine major degradation tasks for evaluation: deblurring, rain removal, denoise, low-light enhancement, moiré patterns removal, haze removal, compression restoration, reflection removal, and deflare, with task-specific English instructions for each model to remove the corresponding degradation.

Unlike full-reference metrics such as PSNR and SSIM [63], which require paired clean reference images for evaluation, RealIR-Bench is built entirely from non-reference images collected from diverse real-world scenarios. In these cases, obtaining perfectly aligned clean targets is infeasible, making conventional full-reference evaluation protocols unsuitable. Therefore, instead of relying on pixel-wise fidelity measures, we adopt a non-reference evaluation framework to assess how well image editing models handle

real-world degradations, with particular emphasis on both degradation removal capability and consistency preservation.

To characterize both restoration effectiveness and the trade-off with content fidelity, we report two metrics: Restoration Score (RS), LPIPS (LPS) [72]. We convert the LPIPS distance into a perceptual similarity score so that higher values indicate better perceptual consistency. After normalizing both RS and LPS to the same scale, the Final Score (FS) is defined as:

$$FS = 0.2(1 - LPS)RS \quad (1)$$

FS jointly reflects restoration improvement and content preservation, and poor performance in either aspect will directly lead to a lower overall score.

Inspired by non-reference evaluation methods such as VIEScore [28], we leverage VLMs to assess Restoration Score. Specifically, we employ Qwen3-VL-8B-Instruct [58] to rate the degradation severity of both degraded images and restored images on a scale from 0 to 5, where 5 indicates no visible degradation, and 0 corresponds to the most severe degradation. The Restoration Score (RS) is defined as the improvement in degradation level after restoration. In other words, it is computed as the difference between the degra-

Table 3. Quantitative comparison on the FoundIR dataset across various real-world degradations. We report PSNR (\uparrow) and SSIM (\uparrow). The best results are highlighted in **bold**, and the second-best results are underlined.

Method	Blur		Rain		Raindrops		Noise		Low-light		Haze		Compression		Average	
	PSNR \uparrow	SSIM \uparrow														
Nano Banana Pro [56]	20.16	0.68	<u>21.55</u>	<u>0.65</u>	<u>23.29</u>	<u>0.66</u>	24.78	0.89	<u>15.73</u>	<u>0.73</u>	<u>17.63</u>	<u>0.50</u>	19.48	0.58	<u>20.37</u>	<u>0.67</u>
GPT-Image-1.5 [45]	13.25	0.41	12.52	0.34	13.89	0.31	14.15	0.68	11.00	0.55	12.39	0.28	13.06	0.39	12.89	0.42
Seedream 4.5 [55]	17.94	0.61	17.61	0.57	18.01	0.58	15.57	0.78	13.64	0.68	15.65	0.44	14.29	0.54	16.10	0.60
LongCat-Image-Edit [57]	18.53	<u>0.65</u>	17.09	0.52	18.22	0.48	19.77	0.81	15.24	0.70	10.52	0.36	15.64	0.47	16.43	0.57
Qwen-Image-Edit-2511 [65]	15.60	0.55	14.68	0.46	15.19	0.42	19.73	0.81	7.13	0.17	7.20	0.34	18.29	0.61	13.98	0.48
FLUX.1-Kontext-dev [30]	10.73	0.41	10.48	0.35	11.25	0.31	15.10	0.69	10.34	0.53	10.74	0.29	10.74	0.34	11.34	0.42
Step1X-Edit [41]	16.38	0.63	19.91	0.63	19.42	0.58	<u>27.18</u>	0.91	15.72	0.70	14.20	0.45	22.81	0.75	19.37	0.66
RealRestorer (ours)	<u>18.99</u>	0.59	23.72	0.71	23.64	0.71	28.15	<u>0.90</u>	17.59	0.77	17.66	0.56	<u>20.40</u>	<u>0.66</u>	21.45	0.70

ation score of the restored image and that of the degraded image. A higher RS indicates greater perceived restoration improvement according to the VLM evaluator.

For consistency evaluation, we aim to measure the model’s ability to preserve the original scene structure, semantic content, and fine-grained details throughout the restoration process. To this end, we employ LPIPS as the evaluation metric to measure the perceptual similarity between the restored images and the degraded inputs. Unlike traditional pixel-level metrics, LPIPS is more sensitive to perceptually relevant discrepancies, including structural deviations and semantic inconsistencies, making it particularly suitable for assessing content preservation before and after restoration.

Table 1 and Table 2 demonstrate the strong restoration capability of RealRestorer. It consistently outperforms existing open-source image editing models and achieves performance comparable to leading closed-source systems. Across all nine tasks, RealRestorer achieves the best performance on deblurring and low-light enhancement and ranks second on moiré pattern removal. Among open-source models, it ranks first on five tasks and second on two, and remains highly competitive on the remaining tasks. Overall, it ranks **first among open-source models** and third overall, narrowing the gap with Nano Banana Pro (first place) to only 0.007 points and surpassing Qwen-Image-Edit-2511 (the second-best open-source model) by 0.019 points. These results indicate that RealRestorer not only effectively removes real-world degradations but also maintains high consistency and fidelity in the restored outputs. As an open-source model, RealRestorer significantly narrows the performance gap between open-source and closed-source systems, while exhibiting strong generalization ability across diverse real-world scenarios. Figure 3 presents qualitative comparisons, further demonstrating that RealRestorer produces visually cleaner and more consistent restoration results compared to other state-of-the-art image editing methods. On real-world degraded images from RealIR-Bench, our model shows strong performance across diverse scenarios. In particular, when handling complex and irregular real-world degradations such as blur and flare, RealRestorer remains highly competitive with leading closed-source models, achieving comparable

visual quality and structural fidelity.

4.3. Extra Benchmark Evaluation and Zero-shot Generalization

To further evaluate restoration performance on a traditional all-in-one benchmark, we additionally evaluate the same set of image editing models on the FoundIR test set [34]. FoundIR contains 20 real-world degradation settings with paired clean references, including 7 isolated degradations (blur, rain, noise, low-light, raindrops, haze, and compression artifacts) and 13 coupled degradation combinations. We report results on the 7 isolated degradation subsets, which also overlap with RealIR-Bench, resulting in a total of 750 paired image pairs with an average resolution of 2514×1516 . For the editing prompt, we use the same prompt set as RealIR-Bench.

Table 3 shows that RealRestorer achieves strong restoration performance on these 7 tasks, obtaining the best PSNR and SSIM on 5 out of 7 degradations. Notably, all image editing models tend to achieve relatively low reference-based metrics, which is consistent with the generative nature of these models that may introduce perceptually plausible yet non-identical details. Benefiting from high-quality synthetic degradation data, RealRestorer achieves a better trade-off while improving content consistency. We further evaluate the generalization ability of RealRestorer via zero-shot experiments on real-world restoration scenarios, including snow removal and old photo restoration. RealRestorer also generalizes well to unseen restoration tasks. Although it is only fine-tuned on a limited set of degradation types, it can still handle other unseen tasks by benefiting from the restoration priors learned during training, while retaining part of the original model’s general image editing capability. More qualitative results, evaluations on additional public benchmarks, and detailed comparisons are provided in Appendix D, together with further visualizations and analysis.

4.4. Ablation and User Studies

We conduct an ablation study on the training data and training stages to examine the necessity of the proposed two-stage training strategy. Specifically, we first train the model on the Synthetic Degradation Data (about 1M samples). As shown in Figure 14, the model acquires basic restoration

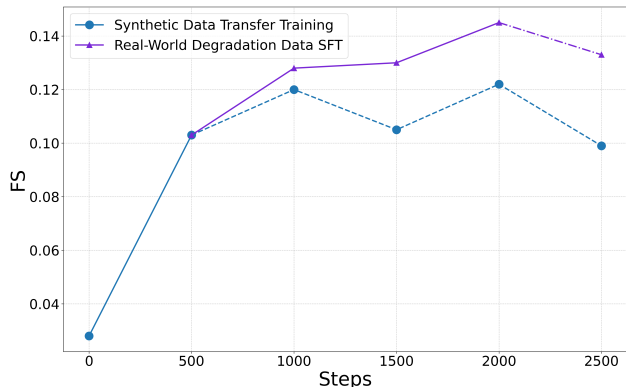


Figure 4. Model performance with varying training steps and training data on RealIR-Bench. The blue line shows transfer training on synthetic degradation data, where the model gradually acquires basic restoration capability. The blue dashed line indicates performance degradation after prolonged training due to the limited diversity of synthetic data. The purple line represents supervised fine-tuning with real-world degradation data, which rapidly improves performance and generalization. The purple dashed segment indicates the onset of overfitting after around 2.5K steps.

capability and reaches a peak FS of 0.122 during the first stage, but still lacks sufficient generalization ability and fails on some rare cases. Moreover, its performance drops significantly after 2.5K steps, which we attribute to the limited diversity of the synthetic data. We further investigate the impact of the Real-World Degradation Data (about 100K samples) in the second stage. After entering this stage, the model quickly surpasses the peak score achieved in the transfer training stage and continues to improve its generalization ability, eventually achieving strong performance at around 2.5K steps. However, beyond this point, the model begins to overfit the Real-World Degradation Data, which motivates us to adopt early stopping. Overall, the two-stage training strategy, together with the combination of synthetic and real-world data, leads to a final model with strong restoration performance and better consistency preservation.

Furthermore, we conduct an ablation study on the Progressively-Mixed training strategy. Without this component, the final FS score decreases by 0.004 points under the same training configuration, confirming its effectiveness. And from a qualitative perspective, the Progressive-Mixed strategy also leads to better preservation of structural consistency and content fidelity, resulting in more visually stable and coherent restoration results. Additional ablation results and analyses are provided in the supplementary materials.

We conduct a user study to evaluate both the reliability of the proposed RealIR-Bench metrics and the perceptual performance of our model from a human perspective. Specifically, we recruit 32 participants to rank 3,200 groups of generated images produced by five high-performing models according to two criteria: restoration quality and content con-

sistency. Specifically, Nano Banana Pro achieves the highest first-ranking rate of 32.02%, followed by GPT-Image-1.5 with 23.83%, while our method attains 21.54%. This trend is consistent with the average overall scores reported in Table 2. Moreover, we perform a statistical analysis of the proposed metrics and observe a moderate alignment with human judgments across all evaluation measures ($p < 0.01$). Further details on the study design, ranking protocol, and statistical analysis are provided in the Appendix F.

5. Limitations and Discussion

Although RealRestorer demonstrates strong generalization across both seen and unseen restoration tasks, we still observe several limitations. First, since the base image editing model relies on a 28-step denoising process, its computational cost remains substantially higher than that of smaller-scale models, which is a common limitation of large-scale image editing models. Second, in cases with strong semantic and physical ambiguity, such as mirror selfies, the model may fail to distinguish true scene content from undesired reflections, a challenge that is also common in other image editing methods. Third, RealRestorer still struggles with extremely severe degradations where reliable pixel evidence is largely missing, and may fail to preserve physically consistent structures such as water reflections.

6. Conclusion

In this paper, we introduce **RealRestorer**, a robust open-source image editing model for complex real-world image restoration. To reduce the synthetic-to-real domain gap, we propose a comprehensive data generation pipeline and a two-stage progressively mixed training strategy that combines synthetic and real-to-clean pairs. We further present **RealIR-Bench**, a non-reference benchmark with authentic degraded images and a VLM-based evaluation framework for real-world restoration. Extensive experiments on many evaluation sets demonstrate that **RealRestorer** achieves open-source state-of-the-art performance across nine restoration tasks, with results highly comparable to leading closed-source commercial systems, and exhibits strong zero-shot generalization to unseen degradations. We will release our model, data synthesis pipeline, and benchmark to support future research in real-world image restoration.

References

- [1] SM Al-Salem, G Abraham, OA Al-Qabandi, and AM Dashti. Investigating the effect of accelerated weathering on the mechanical and physical properties of high content plastic solid waste (psw) blends with virgin linear low density polyethylene (lldpe). *Polymer Testing*, 46:116–121, 2015. 2
- [2] Shuai Bai, Yuxuan Cai, Ruizhe Chen, Keqin Chen, Xionghui Chen, Zesen Cheng, Lianghao Deng, Wei Ding, Chang Gao, Chunjiang Ge, et al. Qwen3-vl technical report. *arXiv preprint arXiv:2511.21631*, 2025. 4
- [3] Arnold O Benz. Flare observations. *Living reviews in solar physics*, 14(1):2, 2017. 2
- [4] Holger Caesar, Varun Bankiti, Alex H Lang, Sourabh Vora, Venice Erin Liong, Qiang Xu, Anush Krishnan, Yu Pan, Giancarlo Baldan, and Oscar Beijbom. nuscenes: A multimodal dataset for autonomous driving. In *Proceedings of the IEEE/CVF conference on computer vision and pattern recognition*, pages 11621–11631, 2020. 2
- [5] Yuanhao Cai, Hao Bian, Jing Lin, Haoqian Wang, Radu Timofte, and Yulun Zhang. Retinexformer: One-stage retinex-based transformer for low-light image enhancement. In *Proceedings of the IEEE/CVF international conference on computer vision*, pages 12504–12513, 2023. 2, 4
- [6] Ke Cheng, Yifan Zhang, Xiangyu He, Weihan Chen, Jian Cheng, and Hanqing Lu. Skeleton-based action recognition with shift graph convolutional network. In *Proceedings of the IEEE/CVF conference on computer vision and pattern recognition*, pages 183–192, 2020. 14
- [7] Yuning Cui, Syed Waqas Zamir, Salman Khan, Alois Knoll, Mubarak Shah, and Fahad Shahbaz Khan. Adair: Adaptive all-in-one image restoration via frequency mining and modulation. In *13th International Conference on Learning Representations, ICLR 2025*, pages 57335–57356. International Conference on Learning Representations, ICLR, 2025. 2
- [8] Peng Dai, Xin Yu, Lan Ma, Baoheng Zhang, Jia Li, Wenbo Li, Jiajun Shen, and Xiaojuan Qi. Video demoireing with relation-based temporal consistency. In *Proceedings of the IEEE/CVF Conference on Computer Vision and Pattern Recognition*, 2022. 15
- [9] Yuekun Dai, Chongyi Li, Shangchen Zhou, Ruicheng Feng, Yihang Luo, and Chen Change Loy. Flare7k++: Mixing synthetic and real datasets for nighttime flare removal and beyond. 2023. 15
- [10] Niranjana Damera-Venkata, Thomas D Kite, Wilson S Geisler, Brian L Evans, and Alan C Bovik. Image quality assessment based on a degradation model. *IEEE transactions on image processing*, 9(4):636–650, 2000. 2
- [11] Alain Dufaux, Laurent Besacier, Michael Ansorge, and Fausto Pellandini. Automatic sound detection and recognition for noisy environment. In *2000 10th European Signal Processing Conference*, pages 1–4. IEEE, 2000. 2
- [12] Patrick Esser, Sumith Kulal, Andreas Blattmann, Rahim Entezari, Jonas Müller, Harry Saini, Yam Levi, Dominik Lorenz, Axel Sauer, Frederic Boesel, et al. Scaling rectified flow transformers for high-resolution image synthesis. In *Forty-first international conference on machine learning*, 2024. 2
- [13] Jan Flusser, Sajad Farokhi, Cyril Höschl, Tomáš Suk, Barbara Zitova, and Matteo Pedone. Recognition of images degraded by gaussian blur. *IEEE transactions on Image Processing*, 25(2):790–806, 2015. 2
- [14] Qiyuan Guan, Qianfeng Yang, Xiang Chen, Tianyu Song, Guiyue Jin, and Jiyu Jin. Weatherbench: A real-world benchmark dataset for all-in-one adverse weather image restoration. In *Proceedings of the 33rd ACM International Conference on Multimedia*, pages 12607–12613, 2025. 6
- [15] Bahadır Gunturk and Xin Li. *Image restoration*. CRC Press, 2018. 2
- [16] Xiaojie Guo and Qiming Hu. Low-light image enhancement via breaking down the darkness. *International Journal of Computer Vision*, 131(1):48–66, 2023. 2
- [17] Yu Guo, Yuan Gao, Yuxu Lu, Huilin Zhu, Ryan Wen Liu, and Shengfeng He. Onerestore: A universal restoration framework for composite degradation. In *European conference on computer vision*, pages 255–272. Springer, 2024. 2, 3, 6
- [18] Jiang Hai, Zhu Xuan, Ren Yang, Yutong Hao, Fengzhu Zou, Fang Lin, and Songchen Han. R2rnet: Low-light image enhancement via real-low to real-normal network. *Journal of Visual Communication and Image Representation*, 90:103712, 2023. 4
- [19] Feng He, Yongjian Zhou, Zefang Ye, Sang-Hyeok Cho, Jihoon Jeong, Xianghai Meng, and Yaguo Wang. Moiré patterns in 2d materials: a review. *ACS nano*, 15(4):5944–5958, 2021. 2
- [20] Kaiming He, Jian Sun, and Xiaoou Tang. Single image haze removal using dark channel prior. *IEEE transactions on pattern analysis and machine intelligence*, 33(12):2341–2353, 2010. 4
- [21] Klaus Hermann. Periodic overlayers and moiré patterns: theoretical studies of geometric properties. *Journal of Physics: Condensed Matter*, 24(31):314210, 2012. 2
- [22] Han Hu, Jiayuan Gu, Zheng Zhang, Jifeng Dai, and Yichen Wei. Relation networks for object detection. In *Proceedings of the IEEE conference on computer*

- vision and pattern recognition, pages 3588–3597, 2018. 2
- [23] Yihan Hu, Jiazhi Yang, Li Chen, Keyu Li, Chonghao Sima, Xizhou Zhu, Siqi Chai, Senyao Du, Tianwei Lin, Wenhai Wang, et al. Planning-oriented autonomous driving. In Proceedings of the IEEE/CVF conference on computer vision and pattern recognition, pages 17853–17862, 2023. 2
- [24] Yi Huang, Jiancheng Huang, Jianzhuang Liu, Mingfu Yan, Yu Dong, Jiayi Lv, Chaoqi Chen, and Shifeng Chen. Wavedm: Wavelet-based diffusion models for image restoration. IEEE Transactions on Multimedia, 26:7058–7073, 2024. 2
- [25] Yukun Huang, Zheng-Jun Zha, Xueyang Fu, Richang Hong, and Liang Li. Real-world person re-identification via degradation invariance learning. In Proceedings of the IEEE/CVF conference on computer vision and pattern recognition, pages 14084–14094, 2020. 2
- [26] Kui Jiang, Zhongyuan Wang, Peng Yi, Chen Chen, Zheng Wang, Xiao Wang, Junjun Jiang, and Chia-Wen Lin. Rain-free and residue hand-in-hand: A progressive coupled network for real-time image deraining. IEEE Transactions on Image Processing, 30:7404–7418, 2021. 2
- [27] KJ Joseph, Salman Khan, Fahad Shahbaz Khan, and Vineeth N Balasubramanian. Towards open world object detection. In Proceedings of the IEEE/CVF conference on computer vision and pattern recognition, pages 5830–5840, 2021. 2
- [28] Max Ku, Dongfu Jiang, Cong Wei, Xiang Yue, and Wenhui Chen. Viescore: Towards explainable metrics for conditional image synthesis evaluation. In Proceedings of the 62nd Annual Meeting of the Association for Computational Linguistics (Volume 1: Long Papers), pages 12268–12290, 2024. 7
- [29] Black Forest Labs. Flux. <https://github.com/black-forest-labs/flux>, 2024. 4
- [30] Black Forest Labs, Stephen Batifol, Andreas Blattmann, Frederic Boesel, Saksham Consul, Cyril Diagne, Tim Dockhorn, Jack English, Zion English, Patrick Esser, et al. Flux. 1 kontekst: Flow matching for in-context image generation and editing in latent space. arXiv preprint arXiv:2506.15742, 2025. 2, 7, 8
- [31] Jaakko Lehtinen, Jacob Munkberg, Jon Hasselgren, Samuli Laine, Tero Karras, Miika Aittala, and Timo Aila. Noise2noise: Learning image restoration without clean data. arXiv preprint arXiv:1803.04189, 2018. 2
- [32] Boyi Li, Wenqi Ren, Dengpan Fu, Dacheng Tao, Dan Feng, Wenjun Zeng, and Zhangyang Wang. Benchmarking single-image dehazing and beyond. IEEE transactions on image processing, 28(1):492–505, 2018. 2
- [33] Boyun Li, Xiao Liu, Peng Hu, Zhongqin Wu, Jiancheng Lv, and Xi Peng. All-in-one image restoration for unknown corruption. In Proceedings of the IEEE/CVF conference on computer vision and pattern recognition, pages 17452–17462, 2022. 2
- [34] Hao Li, Xiang Chen, Jiangxin Dong, Jinhui Tang, and Jinshan Pan. Foundir: Unleashing million-scale training data to advance foundation models for image restoration. In Proceedings of the IEEE/CVF International Conference on Computer Vision, pages 12626–12636, 2025. 2, 3, 4, 6, 8
- [35] Yawei Li, Kai Zhang, Jingyun Liang, Jiezhang Cao, Ce Liu, Rui Gong, Yulun Zhang, Hao Tang, Yun Liu, Denis Demandolx, et al. Lsdir: A large scale dataset for image restoration. In Proceedings of the IEEE/CVF Conference on Computer Vision and Pattern Recognition, pages 1775–1787, 2023. 2
- [36] Jie Liang, Hui Zeng, and Lei Zhang. Efficient and degradation-adaptive network for real-world image super-resolution. In European Conference on Computer Vision, pages 574–591. Springer, 2022. 2
- [37] Jingyun Liang, Jiezhang Cao, Guolei Sun, Kai Zhang, Luc Van Gool, and Radu Timofte. Swinir: Image restoration using swin transformer. In Proceedings of the IEEE/CVF international conference on computer vision, pages 1833–1844, 2021. 2
- [38] Xinqi Lin, Jingwen He, Ziyang Chen, Zhaoyang Lyu, Bo Dai, Fanghua Yu, Yu Qiao, Wanli Ouyang, and Chao Dong. Diffbir: Toward blind image restoration with generative diffusion prior. In European conference on computer vision, pages 430–448. Springer, 2024. 2
- [39] Yaron Lipman, Ricky TQ Chen, Heli Ben-Hamu, Maximilian Nickel, and Matt Le. Flow matching for generative modeling. arXiv preprint arXiv:2210.02747, 2022. 2
- [40] Jiaying Liu, Dejia Xu, Wenhan Yang, Minhao Fan, and Haofeng Huang. Benchmarking low-light image enhancement and beyond. International Journal of Computer Vision, 129(4):1153–1184, 2021. 2
- [41] Shiyu Liu, Yucheng Han, Peng Xing, Fukun Yin, Rui Wang, Wei Cheng, Jiaqi Liao, Yingming Wang, Honghao Fu, Chunrui Han, et al. Step1x-edit: A practical framework for general image editing. arXiv preprint arXiv:2504.17761, 2025. 2, 4, 5, 7, 8
- [42] Ziwei Luo, Fredrik K Gustafsson, Zheng Zhao, Jens Sjölund, and Thomas B Schön. Controlling vision-language models for universal image restoration. arXiv preprint arXiv:2310.01018, 3(8), 2023. 2
- [43] Matthias Minderer, Alexey Gritsenko, and Neil Houlsby. Scaling open-vocabulary object detection, 2023. 3, 14

- [44] Seungjun Nah, Tae Hyun Kim, and Kyoung Mu Lee. Deep multi-scale convolutional neural network for dynamic scene deblurring. In *CVPR*, July 2017. 2
- [45] OpenAI. Introducing 4o image generation, 2025. 2, 7, 8
- [46] William Peebles and Saining Xie. Scalable diffusion models with transformers. In *Proceedings of the IEEE/CVF international conference on computer vision*, pages 4195–4205, 2023. 2, 4
- [47] Dustin Podell, Zion English, Kyle Lacey, Andreas Blattmann, Tim Dockhorn, Jonas Müller, Joe Penna, and Robin Rombach. Sdxl: Improving latent diffusion models for high-resolution image synthesis. *arXiv preprint arXiv:2307.01952*, 2023. 4
- [48] Vaishnav Potlapalli, Syed Waqas Zamir, Salman H Khan, and Fahad Shahbaz Khan. Promptir: Prompting for all-in-one image restoration. *Advances in Neural Information Processing Systems*, 36:71275–71293, 2023. 2
- [49] Alec Radford, Jong Wook Kim, Chris Hallacy, Aditya Ramesh, Gabriel Goh, Sandhini Agarwal, Girish Sastry, Amanda Askell, Pamela Mishkin, Jack Clark, et al. Learning transferable visual models from natural language supervision. In *International conference on machine learning*, pages 8748–8763. PmLR, 2021. 4, 14
- [50] Sudarshan Rajagopalan, Nithin Gopalakrishnan Nair, Jay N. Paranjape, and Vishal M. Patel. Gendeg: Diffusion-based degradation synthesis for generalizable all-in-one image restoration, 2024. 6
- [51] René Ranftl, Katrin Lasinger, David Hafner, Konrad Schindler, and Vladlen Koltun. Towards robust monocular depth estimation: Mixing datasets for zero-shot cross-dataset transfer. *IEEE Transactions on Pattern Analysis and Machine Intelligence*, 44(3), 2022. 3
- [52] Nikhila Ravi, Valentin Gabeur, Yuan-Ting Hu, Ronghang Hu, Chaitanya Ryali, Tengyu Ma, Haitham Khedr, Roman Rädle, Chloe Rolland, Laura Gustafson, et al. Sam 2: Segment anything in images and videos. *arXiv preprint arXiv:2408.00714*, 2024. 3
- [53] Robin Rombach, Andreas Blattmann, Dominik Lorenz, Patrick Esser, and Björn Ommer. High-resolution image synthesis with latent diffusion models. In *Proceedings of the IEEE/CVF conference on computer vision and pattern recognition*, pages 10684–10695, 2022. 2
- [54] Team Seedream, :, Yunpeng Chen, Yu Gao, Lixue Gong, Meng Guo, Qiushan Guo, Zhiyao Guo, Xiaoxia Hou, Weilin Huang, Yixuan Huang, Xiaowen Jian, Huafeng Kuang, Zhichao Lai, Fanshi Li, Liang Li, Xiaochen Lian, Chao Liao, Liyang Liu, Wei Liu, Yanzuo Lu, Zhengxiong Luo, Tongtong Ou, Guang Shi, Yichun Shi, Shiqi Sun, Yu Tian, Zhi Tian, Peng Wang, Rui Wang, Xun Wang, Ye Wang, Guofeng Wu, Jie Wu, Wenxu Wu, Yonghui Wu, Xin Xia, Xuefeng Xiao, Shuang Xu, Xin Yan, Ceyuan Yang, Jianchao Yang, Zhonghua Zhai, Chenlin Zhang, Heng Zhang, Qi Zhang, Xinyu Zhang, Yuwei Zhang, Shijia Zhao, Wenliang Zhao, and Wenjia Zhu. Seedream 4.0: Toward next-generation multimodal image generation, 2025. 7
- [55] Team Seedream, Yunpeng Chen, Yu Gao, Lixue Gong, Meng Guo, Qiushan Guo, Zhiyao Guo, Xiaoxia Hou, Weilin Huang, Yixuan Huang, et al. Seedream 4.0: Toward next-generation multimodal image generation. *arXiv preprint arXiv:2509.20427*, 2025. 7, 8
- [56] Gemini Team, Rohan Anil, Sebastian Borgeaud, Jean-Baptiste Alayrac, Jiahui Yu, Radu Soricut, Johan Schalkwyk, Andrew M Dai, Anja Hauth, Katie Millican, et al. Gemini: a family of highly capable multimodal models. *arXiv preprint arXiv:2312.11805*, 2023. 2, 7, 8
- [57] Meituan LongCat Team, Hanghang Ma, Haoxian Tan, Jiale Huang, Junqiang Wu, Jun-Yan He, Lishuai Gao, Songlin Xiao, Xiaoming Wei, Xiaoqi Ma, Xunliang Cai, Yayong Guan, and Jie Hu. Longcat-image technical report. *arXiv preprint arXiv:2512.07584*, 2025. 2, 4, 6, 7, 8
- [58] Qwen Team. Qwen3 technical report, 2025. 4, 7, 14
- [59] Z-Image Team. Z-image: An efficient image generation foundation model with single-stream diffusion transformer. *arXiv preprint arXiv:2511.22699*, 2025. 4, 6
- [60] Li Tong and JR White. Photo-oxidation of thermoplastics in bending and in uniaxial compression. *Polymer degradation and stability*, 53(3):381–396, 1996. 2
- [61] Xintao Wang, Liangbin Xie, Chao Dong, and Ying Shan. Real-esrgan: Training real-world blind super-resolution with pure synthetic data. In *International Conference on Computer Vision Workshops (ICCVW)*. 4
- [62] Yan Wang, Ling Yang, Xinzhan Liu, and Pengfei Yan. An improved semantic segmentation algorithm for high-resolution remote sensing images based on deeplabv3+. *Scientific reports*, 14(1):9716, 2024. 2
- [63] Zhou Wang, Alan C Bovik, Hamid R Sheikh, and Eero P Simoncelli. Image quality assessment: from error visibility to structural similarity. *IEEE transactions on image processing*, 13(4):600–612, 2004. 7
- [64] Qiang Wen, Yinjie Tan, Jing Qin, Wenxi Liu, Guoqiang Han, and Shengfeng He. Single image reflection removal beyond linearity. In *The IEEE Conference on Computer Vision and Pattern Recognition (CVPR)*, June 2019. 4
- [65] Chenfei Wu, Jiahao Li, Jingren Zhou, Junyang Lin, Kaiyuan Gao, Kun Yan, Sheng ming Yin, Shuai Bai,

Xiao Xu, Yilei Chen, Yuxiang Chen, Zecheng Tang, Zekai Zhang, Zhengyi Wang, An Yang, Bowen Yu, Chen Cheng, Dayiheng Liu, Deqing Li, Hang Zhang, Hao Meng, Hu Wei, Jingyuan Ni, Kai Chen, Kuan Cao, Liang Peng, Lin Qu, Minggang Wu, Peng Wang, Shuting Yu, Tingkun Wen, Wensen Feng, Xiaoxiao Xu, Yi Wang, Yichang Zhang, Yongqiang Zhu, Yujia Wu, Yuxuan Cai, and Zenan Liu. Qwen-image technical report, 2025. [2](#), [6](#), [7](#), [8](#)

Yicheng Zhang, Yiwei Zhang, Yongxin Yan, Kaixing Huang, Weisen Chen, Yongtai Deng, et al. Is nano banana pro a low-level vision all-rounder? a comprehensive evaluation on 14 tasks and 40 datasets. arXiv preprint arXiv:2512.15110, 2025. [2](#)

- [66] Wenhan Yang, Wenjing Wang, Haofeng Huang, Shiqi Wang, and Jiaying Liu. Sparse gradient regularized deep retinex network for robust low-light image enhancement. IEEE Transactions on Image Processing, 30:2072–2086, 2021. [4](#)
- [67] Zemin Yang, Yujing Sun, Xidong Peng, Siu Ming Yiu, and Yuexin Ma. Unidemoiré: Towards universal image demoiréing with data generation and synthesis. In Proceedings of the AAAI Conference on Artificial Intelligence, volume 39, pages 9354–9362, 2025. [4](#)
- [68] Yao Yao, Zixin Luo, Shiwei Li, Tian Fang, and Long Quan. Mvsnet: Depth inference for unstructured multi-view stereo. In Proceedings of the European conference on computer vision (ECCV), pages 767–783, 2018. [2](#)
- [69] Eduard Zamfir, Zongwei Wu, Nancy Mehta, Yuedong Tan, Danda Pani Paudel, Yulun Zhang, and Radu Timofte. Complexity experts are task-discriminative learners for any image restoration. In Proceedings of the Computer Vision and Pattern Recognition Conference, pages 12753–12763, 2025. [2](#)
- [70] Syed Waqas Zamir, Aditya Arora, Salman Khan, Munawar Hayat, Fahad Shahbaz Khan, Ming-Hsuan Yang, and Ling Shao. Multi-stage progressive image restoration. In Proceedings of the IEEE/CVF conference on computer vision and pattern recognition, pages 14821–14831, 2021. [2](#)
- [71] Kai Zhang, Jingyun Liang, Luc Van Gool, and Radu Timofte. Designing a practical degradation model for deep blind image super-resolution. In Proceedings of the IEEE/CVF international conference on computer vision, pages 4791–4800, 2021. [2](#)
- [72] Richard Zhang, Phillip Isola, Alexei A Efros, Eli Shechtman, and Oliver Wang. The unreasonable effectiveness of deep features as a perceptual metric. In Proceedings of the IEEE conference on computer vision and pattern recognition, pages 586–595, 2018. [7](#), [15](#)
- [73] Hao Zhao, Mingjia Li, Qiming Hu, and Xiaojie Guo. Reversible decoupling network for single image reflection removal. In Proceedings of the Computer Vision and Pattern Recognition Conference, pages 26430–26439, 2025. [2](#)
- [74] Jialong Zuo, Haoyou Deng, Hanyu Zhou, Jiaxin Zhu,

Appendix

A. Data Construction Details

A.1. Synthetic Degradation Data

For the Synthetic Degradation Data, we collect the clean image from the internet and synthesize the nine major degradation patterns: blur, rain, noise, low-light, moiré patterns, haze, compression artifacts, reflection, and flare. We will release the pipeline.

A.2. Real-World Degradation Data

For the real-world degradation data, we collect clean images from high-quality open-source image websites, including Pexels and Pinterest, covering six types of degradation: blur, rain, low light, haze, reflection, and flare. These degradation types often exhibit a substantial gap between real-world degradations and synthesized patterns.

Table 4. Semantic prompts used for CLIP-based degradation filtering.

Degradation Type	CLIP Text Prompt
Flare	a photo with lens flare, bright streaks of light
Haze	a hazy photo, foggy atmosphere, low contrast
Rain	a rainy photo with rain streaks or raindrops
Low-light	a dark photo, underexposed, low illumination
Blur	a blurry photo with motion blur or out-of-focus regions
Reflection	a photo with glass or mirror-like reflection artifacts

To construct a high-quality real-world degradation dataset, we first employ the CLIP model [49] to filter images based on degradation-related semantic cues, as shown in Table 4. Second, we apply a watermark detection filter [43] together with Qwen3-VL-8B-Instruct [58] to remove watermarked images and images with insufficient degradation, thereby retaining samples suitable for obtaining paired clean data. After selecting appropriate editing models to generate a large amount of raw paired data, additional filtering is required to remove failure cases. Specifically, we use Qwen3-VL-8B-Instruct to estimate the degradation scores of both the clean and degraded images, and then filter pairs with inconsistent or insufficient score differences, while a skeleton-shift-based method [6] is adopted to remove pixel pairs with alignment errors. Finally, after strictly filtering the raw dataset, we further performed human curation on the remaining subset to construct the final dataset. Three trained human experts participated in the annotation and verification process.

A.3. Training Dataset statistics

Table 5 summarizes the statistics of the two components of our training data across different degradation types. Visual

examples of the data are presented in Figure 5.

Table 5. Statistics of our dataset across different degradation types. The table reports the number of training image pairs from Synthetic Degradation Data and Real-World Degradation Data. The total column indicates the combined number of samples for each degradation category.

Degradation	Synthetic	Real	Total
Rain	84,968	43,415	128,383
Blur	1,014,229	13,458	1,027,687
Low-light	5,000	7,005	12,005
Hazy	103,971	8,147	112,118
Reflection	68,227	7,604	75,831
Flare	59,520	7,956	67,476
Moire	99,085	0	99,085
Noise	64,492	0	64,492
Compression	68,000	0	68,000
Total	1,567,492	87,585	1,655,077

B. Implementation Details

During training, we treat the DiT blocks as trainable components, while freezing both the VAE and text encoders. In the Transfer Training Stage, we train the model using the Synthetic Degradation Dataset, which covers nine degradation types. To balance the learning across tasks, we adopt an average sampling strategy over all nine degradation categories. In this stage, the bucket resolution is fixed at 1024×1024 , and the global batch size is set to 16.

After approximately 500 training steps, the model begins to transfer knowledge from high-level editing capabilities to low-level restoration tasks. However, it still struggles to handle more complex degradations, often producing artifacts in the restored results. To address this limitation, we introduce a Supervised Fine-Tuning Stage. In this stage, we adopt a Progressively-Mixed training strategy, combining Real-World Degradation Data with a small portion of Synthetic Degradation Data. This strategy helps constrain the model toward the data manifold of real-world restoration tasks while retaining the robustness learned from synthetic degradations.

Additionally, we freeze the first one-fourth of the SingleStreamBlocks in the DiT architecture to stabilize training. The global batch size is increased to 32, and a cosine annealing learning rate schedule is applied, where the learning rate gradually decays to zero while maintaining the same initial learning rate as in the first stage. This stage lasts for 1.5K training steps, allowing the model to converge to a balanced and generalizable checkpoint. All experiments are conducted on NVIDIA H800 GPUs, and the entire training process takes approximately one day on 8 H800 GPUs. More detailed training hyperparameters are provided in Table 6.

Table 6. Training hyperparameters used in the two training stages.

Hyperparameters	Transfer Training Stage	Supervised Fine-Tuning Stage
Learning rate	1×10^{-5}	$1 \times 10^{-5} \rightarrow 0$
LR scheduler	Constant	Cosine
Weight decay	0.0	0.01
Gradient norm clip	1.0	1.0
Optimizer	AdamW ($\beta_1 = 0.9, \beta_2 = 0.95, \epsilon = 1e^{-8}$)	
Warm-up steps	100	100
Frozen layers	None	First 1/4 SingleStreamBlocks
Training steps	500	1500
Training samples	1.5M	80K
Resolution	1024×1024	1024×1024
Synthetic : Real data ratio	1 : 0	2 : 8

C. RealIR-Bench and Metrics Details

RealIR-Bench covers diverse real-world degradation scenarios, including blur, rain, noise, low-light, moiré patterns, haze, compression artifacts, reflection, and flare. Example cases from the benchmark are shown in Figure 8.

Specifically, we evaluate models using two complementary metrics: Restoration Score (RS), which reflects the perceptual restoration quality, and LPIPS [72], which measures perceptual similarity to assess consistency after restoration.

C.1. Restoration Score

The Restoration Score (RS) is designed to evaluate the ability of a model to remove degradations without explicitly considering content consistency. Inspired by VIEScore, we employ Qwen3-VL-8B-Instruct as a vision-language evaluator to assess the degradation severity of both degraded images and restored images. The Restoration Score (RS) is then defined as the improvement in the degradation level after restoration. The detailed system instruction for Qwen3-VL-8B-Instruct is shown in the Figure 9.

D. More Qualitative Results and Benchmark Evaluation

We present additional visualization results in the following pages to further demonstrate the strong restoration capability of our model compared with other image editing models on **RealIR-Bench** across nine degradation types.

Furthermore, to evaluate **RealRestorer** on public benchmarks for deflare, reflection removal, and demoiré, we conduct additional experiments on several widely used datasets. For deflare evaluation, we use the Flare-R subset from the Flare7K++ dataset [9], which contains 100 paired real-world flare images. The Flare7K++ dataset combines synthetic and real flare data and provides a comprehensive benchmark for nighttime flare removal tasks.

For moiré pattern removal evaluation, we adopt the

UHDM test set [8], which contains 500 paired real moiré images captured at ultra-high resolution. For reflection removal, we evaluate on the SIR²⁺ benchmark, which includes three subsets: SolidObjectDataset, PostcardDataset, and WildScene, containing 50, 50, and 101 paired images respectively. These datasets include real-world scenes with complex reflective patterns and are widely used for evaluating single-image reflection removal methods. The quantitative comparison results are presented in Table 7. The results show that **RealRestorer** achieves the second-best performance in PSNR and the third-best performance in SSIM on average across the five evaluation datasets.

E. Ablation Study Details

Besides comparing the proposed two-stage training strategy composed of the synthetic degradation transfer training stage and the real-world degradation SFT stage, we further analyze an alternative setting where the model is trained using only real-world degradation data. For a fair comparison, we train the model for the same number of iterations as in the synthetic transfer training stage. At the peak point, the model trained only on real-world data tends to overfit the degradation patterns, which harms the structural consistency of the restored images. This often results in artifacts such as object deformation, body shifting, and unrealistic enhancement. These observations further confirm the importance of the proposed two-stage training strategy.

Specifically, at 2.5K training steps, the model trained with only synthetic degradation data still shows limited ability to handle complex real-world degradations, while the model trained solely on real-world degradation data can partially restore degradations but often fails to preserve content consistency. The model produces overly enhanced results, such as removing natural light sources, as shown in Figure 14. In contrast, our two-stage training strategy effectively balances restoration capability and structural consistency, leading to more stable and generalizable performance.

Table 7. Quantitative comparison on extra public benchmarks for real-world image restoration tasks. We report PSNR (\uparrow) and SSIM (\uparrow). The evaluation is conducted on multiple datasets including **Flare-R** from Flare7K++ for deflare, **UHDM** for moiré pattern removal, and the **SIR²**+ reflection removal benchmark with three subsets: PostcardDataset, SolidObjectDataset, and WildScene. Flare-R contains real captured flare images, while UHDM provides ultra-high-definition paired moiré images. The SIR²+ subsets represent different reflection scenarios with diverse scene contents. The best results are highlighted in **bold**, and the second-best results are underlined.

Method	Flare		Moiré		Refl (Postcard)		Refl (Solid)		Refl (Wildscene)		Average	
	PSNR \uparrow	SSIM \uparrow	PSNR \uparrow	SSIM \uparrow	PSNR \uparrow	SSIM \uparrow						
Nano Banana Pro	25.28	0.889	18.86	<u>0.726</u>	20.11	0.821	24.53	0.880	<u>22.27</u>	0.835	22.21	0.830
GPT-Image-1.5	16.86	0.526	11.84	0.549	13.51	0.465	13.97	0.451	14.59	0.527	14.15	0.504
Seedream 4.5	23.88	0.831	15.30	0.643	<u>21.38</u>	0.807	<u>22.16</u>	0.809	21.45	0.783	20.83	0.775
LongCat-Image-Edit	22.57	0.809	15.79	0.670	20.28	0.706	17.12	0.632	21.28	0.805	19.41	0.724
Qwen-Image-Edit-2511	22.45	<u>0.869</u>	16.07	0.673	21.07	0.839	20.17	<u>0.864</u>	23.77	0.896	20.71	<u>0.828</u>
FLUX.1-Kontext-dev	23.27	0.859	10.36	0.516	13.43	0.428	11.60	0.374	14.62	0.520	14.66	0.539
Step1X-Edit	18.74	0.772	14.31	0.583	19.29	<u>0.841</u>	18.56	0.783	21.12	<u>0.864</u>	18.40	0.769
Ours	22.05	0.745	<u>17.62</u>	0.743	22.67	0.904	20.35	0.797	21.72	0.826	<u>20.88</u>	0.803

F. User Study Details

Our user study evaluates the results of the five best-performing models on **RealIR-Bench**. All the 32 participants receive a brief tutorial beforehand to ensure they understand the task and the evaluation criteria. The interface used in the user study is illustrated in Figure 15. To further analyze the reliability of the proposed metric, we compute the Kendall’s τ_b , Spearman Rank Correlation Coefficient (SRCC), and Pearson Linear Correlation Coefficient (PLCC) between the metric score (FS) and human judgments. These correlation measures are widely used to evaluate the consistency between automatic metrics and human evaluation. The results demonstrate that the proposed metric achieves moderate statistical alignment with human judgments ($p < 0.01$) across all evaluation settings, as shown in Table 8.

Table 8. Consistency evaluation between RS metric and subjective human perception.

Metric	Correlation Coefficient	p -value
Kendall’s τ_b	0.2493	2.96×10^{-124}
SRCC	0.3010	4.62×10^{-128}
PLCC	0.2919	3.21×10^{-120}

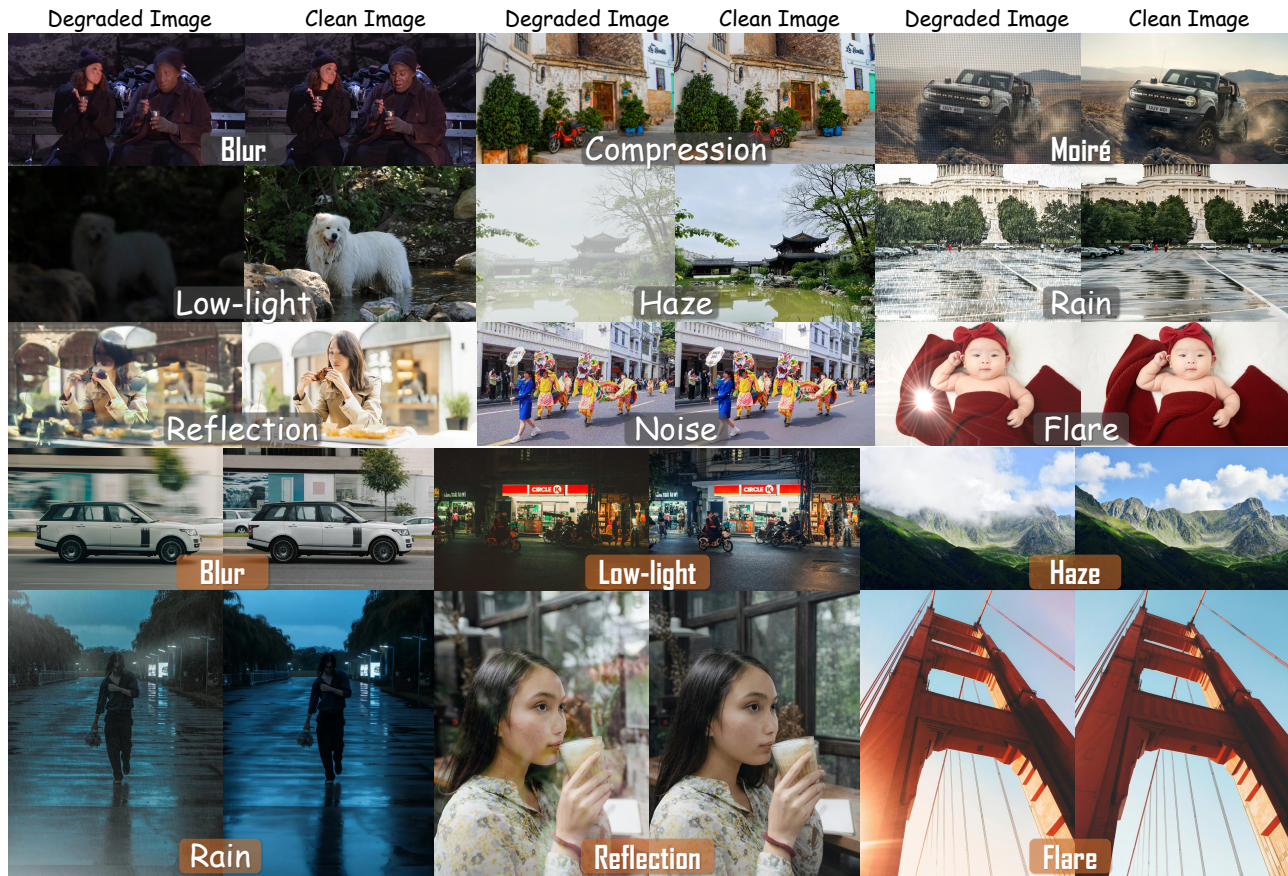


Figure 5. Examples from our training dataset containing both synthetic and real-world degradation pairs. The upper rows with gray labels show synthesized degradations generated by our pipeline, while the bottom rows highlighted with orange labels correspond to real-world degraded images paired with clean references.

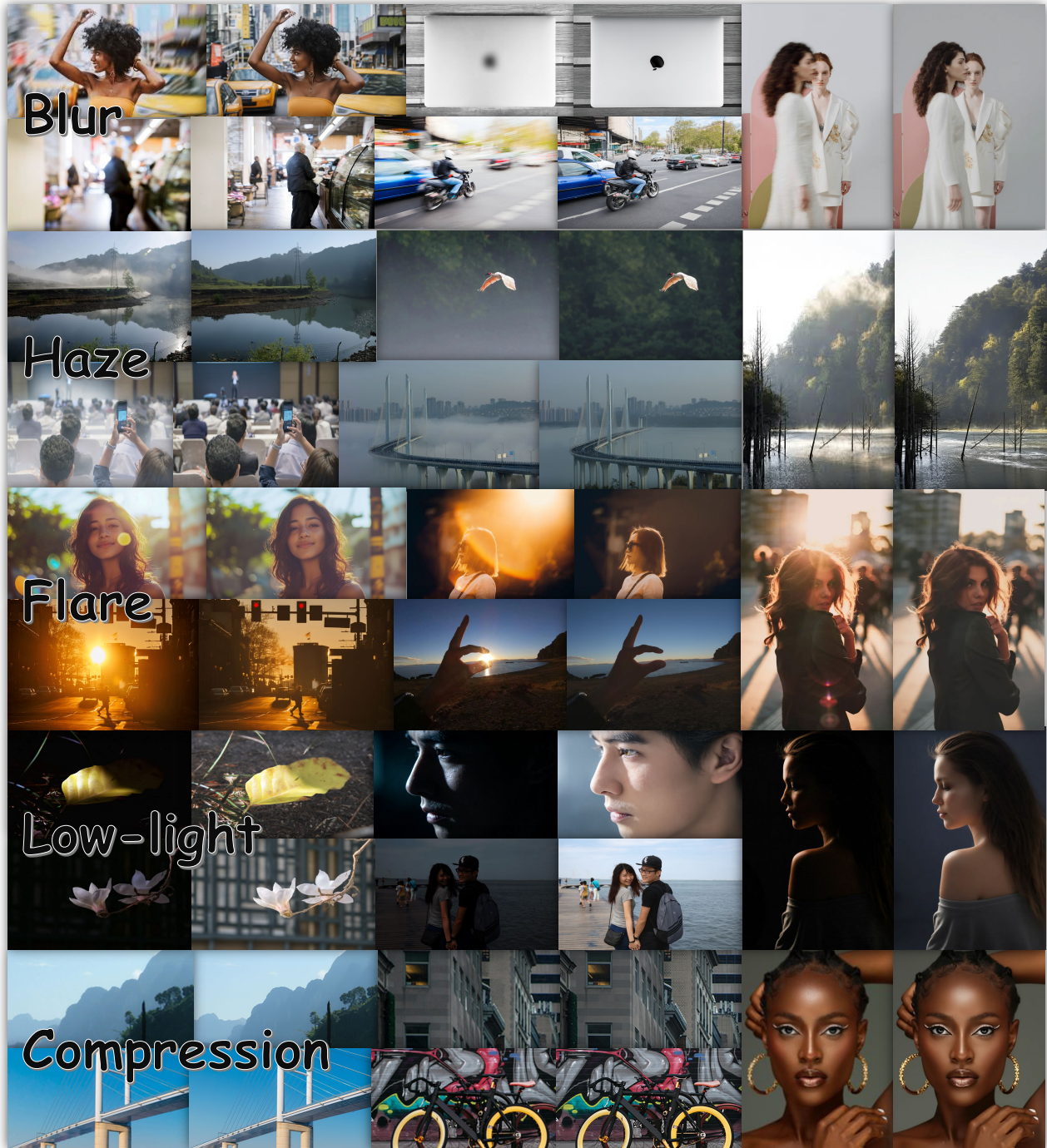


Figure 6. Additional qualitative results of RealRestorer under real-world degradations. Please zoom in for better visualization of details.



Figure 7. Additional qualitative results of RealRestorer under real-world degradations. Please zoom in for better visualization of details.



[Blur] Please deblur the image and make it sharper.
 请将图像去模糊，变得更清晰。



[Compression] Please restore the image clarity and artifacts.
 请修复图像清晰度和伪影。



[Moiré] Please remove the moiré patterns from the image.
 请将图像中的摩尔条纹去除。



[Low-light] Please restore this low-quality image, recovering its normal brightness and clarity.
 请修复这张低质量图像，恢复其正常的亮度和清晰度。



[Noise] Please remove noise from the image.
 请修复请去除图像中的噪声。



[Flare] Please remove the lens flare and glare from the image.
 请去除图像中的光晕和炫光。



[Haze] Please dehaze the image.
 请将图像去雾。



[Rain] Please remove the rain from the image and restore its clarity.
 请去除图像中的雨水并恢复图像清晰度。



[Reflection] Please remove the reflection from the image.
 请移除图像中的反光。

Figure 8. Examples from our RealIR-Bench. Each degradation category is evaluated using a fixed bilingual prompt.

Instruction for Degradation Evaluation

- **Degradation Evaluation:** You will evaluate whether an image exhibits the degradation type {task} and determine its severity level. The assessment should focus exclusively on the specified degradation type, while ignoring unrelated image-quality issues, semantic content, and aesthetic preference. Your goal is to provide a consistent and objective judgment of how strongly the target degradation affects the image.
- **Evaluation Procedure:**
 1. Divide the image into several local regions (e.g., a 3×3 grid) to ensure a systematic inspection.
 2. Examine each region carefully and identify whether the degradation type {task} is present.
 3. Estimate both the severity of the degradation and the proportion of the image area that is affected.
 4. Summarize the regional observations into a single overall score that best reflects the image-level degradation.
 5. If the degradation is spatially uneven, place greater emphasis on the regions that are more strongly affected.
 6. For borderline cases, choose the nearest score level based on the dominant visual impression.
 7. Do not output any intermediate reasoning, explanation, or analysis.
- **Scoring Scale (1–5):** Use the following scale to measure the severity of the target degradation. Higher scores indicate cleaner images with less visible degradation, while lower scores indicate stronger and more widespread corruption.
 - 5 = No {task}; the image is essentially clean with no noticeable degradation.
 - 4 = Mild degradation; only a small portion of the image is affected ($\leq 20\%$ area), and the overall visual quality remains largely intact.
 - 3 = Moderate degradation; the degradation is clearly visible and affects a noticeable part of the image (20–50% area).
 - 2 = Severe degradation; the corruption is strong and influences a large portion of the image (50–80% area).
 - 1 = Extreme degradation; the degradation dominates most of the image ($> 80\%$ area) and seriously harms visual quality.
- **Output Format:** Return only in the format “Degradation Score: <1–5>”.

Figure 9. System instruction used for degradation evaluation.



[Blur] Please deblur the image and make it sharper.



[Compression] Please restore the image clarity and artifacts.



[Flare] Please remove the lens flare and glare from the image.



[Moiré] Please remove the moiré patterns from the image.



[Haze] Please dehaze the image.



[Low-light] Please restore this low-quality image, recovering its normal brightness and clarity.



[Noise] Please remove noise from the image.



[Rain] Please remove the rain from the image and restore its clarity.



[Reflection] Please remove the reflection from the image.

Figure 10. More qualitative comparison results on RealIR-Bench. Zoom in to see more details.



[Blur] Please deblur the image and make it sharper.



[Compression] Please restore the image clarity and artifacts.



[Flare] Please remove the lens flare and glare from the image.



[Moiré] Please remove the moiré patterns from the image.



[Haze] Please dehaze the image.



[Low-light] Please restore this low-quality image, recovering its normal brightness and clarity.



[Noise] Please remove noise from the image.



[Rain] Please remove the rain from the image and restore its clarity.



[Reflection] Please remove the reflection from the image.

Figure 11. More qualitative comparison results on RealIR-Bench. Zoom in to see more details.

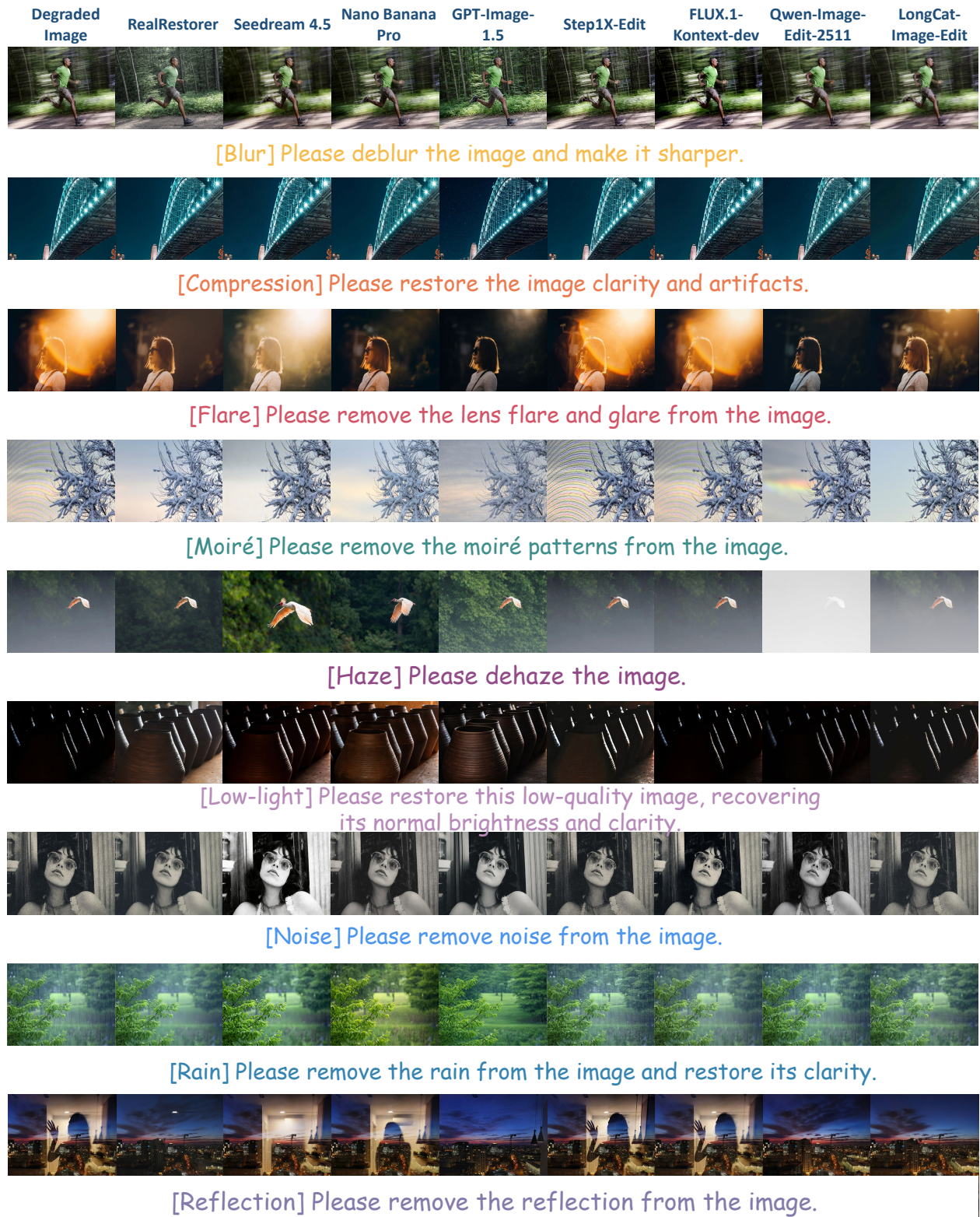


Figure 12. More qualitative comparison results on RealIR-Bench. Zoom in to see more details.



[Blur] Please deblur the image and make it sharper.



[Compression] Please restore the image clarity and artifacts.



[Flare] Please remove the lens flare and glare from the image.



[Moiré] Please remove the moiré patterns from the image.



[Haze] Please dehaze the image.



[Low-light] Please restore this low-quality image, recovering its normal brightness and clarity.



[Noise] Please remove noise from the image.



[Rain] Please remove the rain from the image and restore its clarity.



[Reflection] Please remove the reflection from the image.

Figure 13. More qualitative comparison results on RealIR-Bench. Zoom in to see more details.



Figure 14. Qualitative comparison of different training strategies. Models trained only with synthetic degradation data show limited ability to restore complex real-world degradations. In contrast, models trained solely on real-world degradation data tend to overfit, which may harm structural consistency. Our two-stage training strategy effectively balances restoration capability and content consistency.

Instruction: Please restore this low-quality image, recovering its normal brightness and clarity.

Scoring Dimensions

Enhancement Capability:

Does the output image show clear enhancement compared to the low-quality input image?

Scene Consistency:

Does the enhanced image preserve the original scene content, such as characters, objects, and overall layout?

Overall Quality:

Holistic visual quality and usability of the result (clarity, naturalness, and absence of artifacts).

Scoring Rules (1–5, 1 = Poor, 5 = Excellent)

Enhancement Capability:

1: No meaningful enhancement or the image quality becomes worse.

2–3: Partial improvement, but noticeable degradation or incomplete enhancement remains.

4–5: Clear and effective enhancement with substantial improvement over the input image.

Scene Consistency:

1: Major inconsistency; the scene or key elements are significantly altered or replaced.

2–3: Generally similar but with noticeable inconsistencies (e.g., identity changes, object shifts, or missing elements).

4–5: The scene and key elements remain consistent with the input image.

Overall Quality:

1: Very poor visual quality or severe artifacts.

2–3: Acceptable but with visible flaws or unnatural effects.

4–5: High visual quality, natural appearance, and minimal artifacts.

General Scoring Principles

Absolute Quality: Focus on the actual visual quality of the result. Do not intentionally spread scores just to create differences between methods.

Use the Full Scale: Please utilize the entire 1–5 rating range when appropriate.

Weakest-Link Principle: If a critical failure occurs in any key aspect (e.g., the degradation is removed but the scene or identity changes completely), the final score should be significantly reduced.

Input image



A generated image



B generated image



C generated image



D generated image



E generated image



A score:

B score:

C score:

D score:

E score:

Figure 15. User study interface used to evaluate the restoration results. Participants are presented with one degraded input image and five restored results generated by different models and are asked to rate them based on restoration quality and consistency.